Journal of Fluorine Chemistry 222–223 (2019) 81–89

Contents lists available at ScienceDirect

Journal of Fluorine Chemistry

journal homepage: www.elsevier.com/locate/fluor

High surface area chromium(III) fluoride – Preparation and some properties

Gašper Tavčar, Tomaž Skapin*

Department of Inorganic Chemistry and Technology, Jožef Stefan Institute, Jamova 39, SI-1000 Ljubljana, Slovenia

ARTICLE INFO

Dedicated to Prof. Dr. Erhard Kemnitz, recipient of the 2018 ACS Award for Creative Work in Fluorine Chemistry.

Keywords:
Chromium fluoride
Chromium fluoride oxide
High surface area
Nanostructure
Acidity
Catalysis

ABSTRACT

Reaction of hydrated hydrazinium fluorochromate(III), $[N_2H_6][CrF_5]\cdot H_2O$, with fluorine ($F_2$) in anhydrous hydrogen fluoride (aHF) medium at room temperature yields completely amorphous CrF_3-based materials with exceptionally high specific surface areas of 180–420 $m^2\,g^{-1}$ (HS-CrF_3). The stepwise reaction starts with the oxidative decomposition of the cationic part of the precursor with F_2 that gives a CrF_3 intermediate with low surface area. In the following step, part of Cr^{3+} is oxidized to $Cr^{>3+}$, and in the presence of residual H_2O/$[H_3O]^+$ species $Cr^{>3+}$ fluoride oxides are formed. Formation of volatile chromium compounds, mainly CrO_2F_2, is apparently the key step in HS-CrF_3 formation. Removal of these components from the final product reduces the oxygen content, and generates microporosity. The HS-CrF_3 materials are completely amorphous with a bulk composition that is close to stoichiometric CrF_3. Small amounts of $Cr^{>3+}$ and oxygen in the final product very likely originate from the retained non-volatile $CrOF_3$. The HS-CrF_3 materials are Lewis acids and exhibit a high reactivity towards chlorofluorocarbons (CFCs) evidenced by substantial F/Cl exchange between CFCs and the solid fluoride. High reactivity of these new materials can be ascribed to their nanoscopic nature, exceptionally high surface area, and low levels of impurities. As such, they represent an interesting new class of benchmark fluoride materials applicable in fluorocarbon chemistry.

1. Introduction

Use of chromium-based solid catalysts in fluorocarbon chemistry has a long history [1–3]. Initially, these materials were used as heterogeneous fluorination catalysts, mainly for the production of minor amounts of highly fluorinated chlorofluorocarbons (CFCs) from the C_2 series. With the worldwide adoption of the Montreal Protocol in the late 1980s, interest for this type of heterogeneous catalysts strongly increased. This was the result of a pressing need to develop effective catalytic processes for large-scale production of substances with lower or zero ozone depletion potentials (ODPs), i.e. hydrochlorofluorocarbons (HCFCs), or hydrofluorocarbons (HFCs) [2–6]. Especially some of the HFCs were at that time considered as ideal drop-in replacements for the banned CFC refrigerants. Later on, increasing restrictions and bans were imposed also on the use of HFC refrigerants because of the high global warming potentials (GWPs) of these compounds. Currently, hydrofluoroolefins (HFOs), which exhibit very low GWPs and have a zero ODP, represent the most perspective working replacements for HFCs. For this reason, syntheses of technically relevant HFOs are under intense investigation [7]. Chromium-based catalysts are extensively employed also in this type of reactions, e.g. [8–14].

The pertinent heterogeneous reactions of fluorocarbons are almost exclusively performed on fluorinated chromia (F-Cr_2O_3) catalysts. As a rule, such catalysts are derived from various Cr_2O_3 precursors that are treated at moderate temperatures with gaseous fluorinating agents, like HF, HFCs, CFCs, etc. Such treatment, ordinarily termed “activation”, dehydoxylates and dehydrates the surface, and leads to an at least partial replacement of oxygen with a more electronegative fluorine, which in turn results in an increased Lewis acidity of metal sites. Another process, which can further improve the activity of F-Cr_2O_3, is the in-situ reduction of $Cr^{>3+}$ sites, which are frequently found in Cr_2O_3 precursors, with reductants like HFCs, HCFCs, H_2, or CO. Activation processes leading to catalytically active F-Cr_2O_3 were extensively investigated and are summarized in [2]. As generally accepted, the catalytically active sites in F-Cr_2O_3 are associated with the Cr^{3+} ions being in distorted fluoride-oxide or mixed halide-oxide environments, e.g. CrO_xF_y or $CrO_xF_yCl_z$ [15].

As detailed in [2], formation of the fluoride phase in gas phase fluorinations of Cr_2O_3 is thermodinamically much less favoured as in similar fluorinations of alumina (Al_2O_3) precursors. For these reasons, the Cr_2O_3 substrates undergo only partial fluorination, whereas bulk AlF_3 phases are readily formed when Al_2O_3 is treated under comparable fluorination conditions. Noticeable differences between the

* Corresponding author.
E-mail address: tomaz.skapin@ijs.si (T. Skapin).

https://doi.org/10.1016/j.jfluchem.2019.04.019
Received 4 March 2019; Received in revised form 21 April 2019; Accepted 29 April 2019
Available online 01 May 2019

composition and some other properties of fluorinated Al_2O_3 and Cr_2O_3 were clearly demonstrated in a comparative study of these materials [16].

Fluorination of Cr_2O_3 to F-Cr_2O_3 strongly depends on the nature of the applied fluorinating agent, on temperature, and on the characteristics of the Cr_2O_3 substrate. Although the data on fluorine contents in F-Cr_2O_3 catalysts are frequently lacking, the reported values indicate a very broad range of compositions, ranging from a few percent [16] to 40 mass% of fluorine [8]. Most frequently, the fluorine content is within the range of 10–20 mass%, which roughly corresponds to a 14–30% molar conversion of the precursor Cr_2O_3 to CrF_3. Because of a partial fluorination, F-Cr_2O_3 materials may retain a significant part of the original morphology of the Cr_2O_3 precursors. Surface area and porosity of F-Cr_2O_3 can therefore be tailored to some extent by selecting Cr_2O_3 precursors with adequate topology. Majority of F-Cr_2O_3 materials, which were prepared from conventional Cr_2O_3 precursors, exhibit surface areas in the 30–60 $m^2 g^{-1}$ range. In some cases, surface areas larger than 100 $m^2 g^{-1}$ were obtained by fluorination of atypical Cr_2O_3 precursors, like doped Cr_2O_3 [9,12], Cr_2O_3 pre-mixed with silica (SiO_2) [17,18], or Cr_2O_3 aerogels and xerogels derived from CrO_3 and alcohols [16,19,20]. Especially the latter approach allowed the preparation of F-Cr_2O_3 materials with extraordinarily high surface areas of 210–370 $m^2 g^{-1}$.

In contrast to the widely investigated F-Cr_2O_3 catalysts, application of catalysts based on pure CrF_3 is rather scarce. Well-defined α- and β-CrF_3 phases were occasionally used as fully fluorinated reference materials in comparative studies aimed to elucidate the structure and composition of the possible catalytically active phases present in F-Cr_2O_3. The indicated CrF_3 phases were usually prepared by a strictly controlled thermal decomposition of $[NH_4]_3[CrF_6]$ and exhibited surface areas in the range of 6–74 $m^2 g^{-1}$ [1,16,21,22].

In the last two decades, nanostructured stoichiometric metal fluorides with uncommonly high surface areas (HS-fluorides) received considerable attention, particularly the technically relevant HS-AlF_3 and HS-MgF_2 materials with surface areas well above 100 $m^2 g^{-1}$ [23,24]. Much less attention was devoted to HS-CrF_3 materials. The purely inorganic route to HS-fluorides was originally developed for the preparation of HS-AlF_3 with surface areas of up to 300 $m^2 g^{-1}$ [24,25]. This synthetic approach was based on the decomposition of hydrazinium fluoroaluminate(III) by fluorine (F_2) at room temperature in liquid anhydrous hydrogen fluoride (aHF) medium. As briefly noted in [24], similar treatment of fluorochromate(III) precursors led, in some cases, to remarkably pure amorphous CrF_3 with surprisingly high surface areas, comparable to those observed in HS-AlF_3. It should be noted that earlier thermoanalytical investigations indicated that hydrazinium fluorocromates thermally decompose at around 830 K to give, as stated, an impure CrF_3 [26] or a pure rhombohedral CrF_3 [27].

Preliminary findings about the feasible formation of pure HS-CrF_3 prompted a more systematic and detailed investigation of this rather complex reaction system. This contribution describes the key preparation parameters and the most likely reaction schemes that lead to the formation of HS-CrF_3. Some characteristics of this uncommon type of CrF_3 material, presented here, can be directly related to its distinctive nanostructure, amorphous nature, and unusually high surface area.

2. Results and discussion

2.1. Synthesis

Successful introduction of the inorganic route to HS-AlF_3 [24,25], which involves the decomposition of adequate precursors under homogeneous conditions by the oxidative action of fluorine at or slightly above room temperature, afforded an alternative way to some other fluorides, like CrF_3, GaF_3, FeF_3, and MgF_2. However, preliminary screening of these reactions showed that, with the exemption of CrF_3, all other fluorides had much lower surface areas than HS-AlF_3 [24]. For CrF_3, the preliminary results were ambiguous since surface areas of products from different runs scattered from below 10 to more than 300 $m^2 g^{-1}$. Although the reasons for so large differences were not entirely clear at that time, formation of some products with very high surface areas gave a clear indication that previously unknown HS-CrF_3 materials could be accessible by this means.

Table 1
Surface areas of products after decomposition of various hydrazinium fluorochromates(III) with fluorine in liquid HF medium.

Starting substance	BET surface area ($m^2 g^{-1}$)
$[N_2H_5]_3[CrF_6]$	7–10
$[N_2H_6][CrF_5]\cdot H_2O$ (old)	11
$[N_2H_6][CrF_5]\cdot H_2O$ (fresh)	180–420
$[N_2H_6][CrF_5]\cdot H_2O$ (fresh, H_2 at 293 K)	247

Further investigations of the decomposition reactions, which were all performed with the synthetic protocol detailed in Section 4, clearly demonstrated the key role of the fluorochomate(III) precursors on the surface areas of solid products. Surface areas of typical products obtained from various fluorochomate(III) precursors are compared in Table 1. In the initial decomposition experiments, the anhydrous fluorochromate(III), $[N_2H_5]_3[CrF_6]$, was used as a precursor in analogy with the anhydrous fluoroaluminate(III), $[N_2H_6][AlF_5]$, which was effectively used in the preparation of HS-AlF_3 [25]. However, the resulting surface area of 7 $m^2 g^{-1}$ for the chromium product was comparably very low. Products with similarly low surface areas, i.e. 11 $m^2 g^{-1}$, were initially obtained also from the hydrated precursor, $[N_2H_6][CrF_5]\cdot H_2O$. In both cases, there were some indications that under the applied reaction conditions the decomposition was not complete. In addition, in the initial tests the applied $[N_2H_6][CrF_5]\cdot H_2O$ precursors were taken from old batches, which could have deteriorated over time. To exclude any uncertainties about the precursor, the decomposition tests were repeated with freshly synthesized $[N_2H_6][CrF_5]\cdot H_2O$. With such precursors, oxidative decomposition with fluorine yielded CrF_3 materials with extraordinarily high surfaces areas in the range of 180–420 $m^2 g^{-1}$. In addition, the surface area of these materials was not affected by post-treatment with hydrogen, H_2, at room temperature aimed to reduce the $Cr^{>3+}$ species (Table 1). Further work on HS-CrF_3 materials was therefore focused on the oxidative decomposition of $[N_2H_6][CrF_5]\cdot H_2O$. In order to clarify and optimize this preparation procedure, several preparation runs were performed with rather good repeatability. Surface areas of the so-obtained HS-CrF_3 products were ordinarily within the 300 ± 20 $m^2 g^{-1}$ range. Indicative chemical compositions of a representative HS-CrF_3 in different stages of preparation and post-treatment are given in Table 2.

After completing the reaction, the liquid aHF medium and other volatiles were removed from the reaction vessel by pumping on a vacuum line at room temperature. The mass of the isolated raw solid products was always higher than that expected for the neat stoichiometric conversion to CrF_3 (4), and a substantial surplus of fluorine (F/Cr > 3) was found by chemical analysis, as shown for a raw product in Table 2. This indicated the presence of some impurities. For this reason, raw products were routinely conditioned (dried) under dynamic vacuum at 523 K for at least 20 h. The associated mass losses were in the range 10–30%. Chemical analyses of the desorbed compounds, e.g. F_t, 82.3 mass%, and Cr_t, 2.9 mass%, showed, that the desorbate consists mainly of HF and of a smaller amounts of volatile chromium compounds. The dried products were typical HS-CrF_3 materials with a F/Cr ratio remarkably close to 3 (Table 2). This indicates that treatment in vacuo effectively removes the residual volatile components from the raw products and leaves an almost pure amorphous CrF_3 with exceptionally high surface area. Raman spectra of the raw product before and after vacuum treatment at 523 K, presented in Fig. 1, are consistent with these observations. Bands at 286, 709, and 990 cm^{-1} in the

Table 2
Surface area and composition of a typical HS-CrF_3 formed by the oxidative decomposition of $[N_2H_6][CrF_5]\cdot H_2O$ by F_2.

	Surface area ($m^2\,g^{-1}$)	Component (mass%)							Cr : F : (Cl) / (Cr : (F + Cl))
		Cr_t	Cr^{6+}	F_t^- [a]	Cl_t^-	$[NH_4]^+$	PTFE[b]	Total	
Raw product	/	40.8	3.2	53.2	/	0.4	2.3	96.7	1 : 3.57
HS-CrF_3 Dried at 523 K	284	46.6	1.4	51.0	/	< 0.1[e]	1.9	99.5	1 : 3.00
HS-CrF_3 + CCl_2F_2[c]	169	41.4	0.15	35.3	20,6	/	2.0	99.3	1 : 2.33 : (0.73) / (1 : (3.06))
HS-CrF_3 + $CClF_2CCl_2F$[c]	193	44.2	/	43.1	8,1	/	2.0	97.4	1 : 2.67 : (0.27) / (1 : (2.94))
HS-CrF_3 + acetone[d]	/	37.8	0.0	41.4	/	/	/	79.2	1 : 3.00

[a] Calculated F_t^- content in CrF_3 is 52.29 mass%.
[b] Polytetrafluoroethylene (PTFE) shavings from the attrition of PTFE-coated stir bar (see Section 4).
[c] After catalytic tests with dichlorodifluoromethane at 573 K (CCl_2F_2), or with 1,1,2-trichlorotrifluoroethane at 623 K ($CClF_2CCl_2F$).
[d] Treated with acetone at 523 K.
[e] Below detection limit.

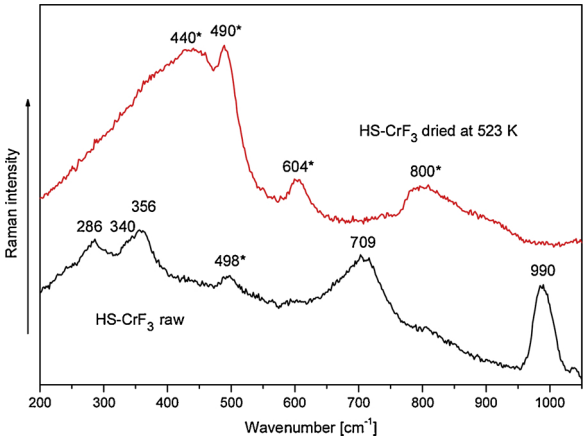

Fig. 1. Raman spectra of the raw HS-CrF_3 product isolated at room temperature (bottom), and of the raw product dried in vacuo at 523 K (top); bands marked with asterisk (*) are from the fused quartz capillary.

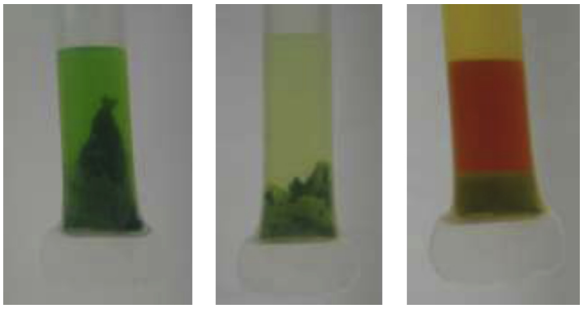

Fig. 2. Discernible visual changes during the reaction of the $[N_2H_6][CrF_5]\cdot H_2O$ precursor with F_2 in liquid aHF at room temperature: precursor in the aHF medium with no F_2 added (left), decomposition to CrF_3 (middle), formation of the CrO_2F_2 by-product (right).

spectrum of the raw product isolated at room temperature (Fig. 1, bottom) match quite well the most intense bands at 275, 708, and 995 cm^{-1}, reported for liquid chromyl fluoride [28], CrO_2F_2. The relatively intense band at 709 cm^{-1}, assigned to the symmetric ν(Cr–F) mode of terminal fluorine atoms, indicates that the residual CrO_2F_2 in the raw product is primarily monomeric. Formation of CrO_2F_2 is also evident from the very characteristic orange coloration of the aHF liquid phase during the reaction of $[N_2H_6][CrF_5]\cdot H_2O$ with F_2 (Fig. 2), as detailed in the next Section. It is therefore very likely that CrO_2F_2 is the major side product of $[N_2H_6][CrF_5]\cdot H_2O$ decomposition although the formation of other $Cr^{>3+}$ fluorides or fluoride oxides, like CrF_4, CrF_5, $CrOF_4$, or $CrOF_3$, cannot be ruled out. However, the presence of an intense broad band at about 990 cm^{-1}, assigned to symmetric ν(Cr–O) modes, suggests that $Cr^{>3+}$ fluoride oxides are the predominant class of side products.

Still, observed Raman bands are relatively broad and the strongest bands of both fluoride oxides, $CrOF_4$ and $CrOF_3$ [6,29,30] are positioned close to those of CrO_2F_2 which can lead to substantial overlapping. As an exemption, the band at 356 with a shoulder at 340 cm^{-1} could be tentatively attributed to $CrOF_3$ [30]. On the other side, Raman spectra of the final products, i.e. raw products conditioned in vacuo at 523 K (Fig. 1, top), do not exhibit any detectable peaks that could be attributed to chromium compounds. The observed pattern with bands at 440, 490, 604, and 800 cm^{-1} is from the quartz capillary and it perfectly matches the reported Raman spectrum of fused silica [31]. Raman spectroscopy evidences therefore a quantitative removal of volatile chromium compounds during vacuum treatment. Main side product is the volatile CrO_2F_2. Identification of other by-products that could be possibly formed, e.g. the volatile $CrOF_4$ or CrF_5, or the non-volatile $CrOF_3$ or CrF_4, is much less reliable. In comparison to CrO_2F_2, concentration of these components is expected to be much lower, and, if present, they are dispersed within the highly amorphous HS-CrF_3 matrix. In addition, the HS-CrF_3 materials are completely amorphous even on the nanoscale, as noted before [24]. Investigation of such disordered materials by means of X-ray diffraction is therefore not feasible.

Determination of Cr^{6+} (Table 2) in the raw products is an additional proof that the decomposition of $[N_2H_6][CrF_5]\cdot H_2O$ with F_2 is accompanied by some oxidation of the initial Cr^{3+} to $Cr^{>3+}$states. In line with the Raman observations, amount of Cr^{6+} is considerably diminished after conditioning in vacuo due to the removal of volatile $Cr^{>3+}$ compounds, mainly CrO_2F_2. The remaining Cr^{6+} in dried HS-CrF_3 may be tentatively associated with $CrOF_3$, which has a polymeric structure and is non-volatile [30] under the applied vacuum treatment conditions. The amount of $CrOF_3$ can be estimated indirectly by taking into account the stoichiometry of its disproportionation in water [30]:

$$3Cr^{5+} \rightarrow 2Cr^{6+} + Cr^{3+} \quad (1)$$

For the dried HS-CrF_3, specified in Table 2, the determined Cr^{6+} value corresponds therefore to a calculated $CrOF_3$ content of 5.0 mass %, which in turn corresponds to 0.6 mass% of oxygen. It is worth noting that the latter value is in reasonable agreement with the missing 0.5 mass% in the total mass balance. For the reasons given above, these levels of $CrOF_3$ are apparently not detectable by Raman spectroscopy.

In the preparation of HS-AlF_3, the non-volatile ammonium fluoroaluminate, $[NH_4][AlF_4]$, was the major by-product originating from the incomplete decomposition of the hydrazinium precursor (3) [25]. Even at the percent levels, the residual $[NH_4]^+$ strongly impaired the catalytic behaviour of HS-AlF_3 materials. Much lower levels of $[NH_4]^+$ were found in the current raw chromium products (Table 2). Further reduction of the $[NH_4]^+$ content was observed after drying in vacuo at 523 K. Such behaviour indicates that the residual $[NH_4]^+$ is very likely in the form of a volatile ammonium fluoride, $[NH_4]F$, since the

ammonium fluorochromate(III), $[NH_4]_3[CrF_6]$, starts to decompose above 673 K [22]. These findings also suggest that in these reaction systems the $[NH_4]^+$ species are almost entirely decomposed.

2.2. Possible reaction scheme

The decomposition reaction of hydrazinium fluorometallates with F_2 was originally developed for the formation of HS-AlF_3 materials from the anhydrous $[N_2H_6][AlF_5]$ precursor [24,25]:

$$[N_2H_6][AlF_5] + 2F_2 \rightarrow AlF_3 + N_2 + 6HF \quad (2)$$

Main side reaction was the formation of $[NH_4][AlF_4]$ due to the incomplete decomposition:

$$2[N_2H_6][AlF_5] + F_2 \rightarrow 2[NH_4][AlF_4] + N_2 + 4HF \quad (3)$$

Since the anhydrous hydrazinium fluorochromate(III) yielded solid products with very low surface area, current work was focused on the decomposition of the hydrated precursor, $[N_2H_6][CrF_5]\cdot H_2O$. Total decomposition of the latter should, in analogy with the aluminium system (2), give CrF_3 as the only solid product:

$$2[N_2H_6][CrF_5]\cdot H_2O + 6F_2 \rightarrow 2CrF_3 + 2N_2 + O_2 + 16HF \quad (4)$$

However, distinctive changes in the colour of the solid and liquid phases (Fig. 2) indicate that reaction is more complex as it could be inferred from (4). In contrast to the aluminium systems, decomposition also involves some oxidation of Cr^{3+} to $Cr^{>3+}$, and formation of various chromium fluoride oxides. Very characteristic colour (Fig. 2 right) and Raman spectra of the raw decomposition product (Fig. 1) are consistent with the formation of CrO_2F_2, which appears to be the prevalent side product. It seems that formation of volatile by-products is an important step towards the preparation of HS-CrF_3 materials.

Decomposition goes through distinctive consecutive stages, which can be followed visually (Fig. 2). In the first step, the intensively green solution of the $[N_2H_6][CrF_5]\cdot H_2O$ precursor in aHF (Fig. 2 left) is slowly discoloured to a slightly greenish liquid, while the dark-green crystalline starting material slowly changes into a grass-green solid (Fig. 2 middle). Reaction is between F_2 and $[N_2H_6][CrF_5]\cdot H_2O$ solvated in aHF. Within the initial stage, a strongly exothermic reaction between the strong oxidant F_2 and the strongly reducing $[N_2H_6]^{2+}$ cation predominates:

$$[N_2H_6][CrF_5]\cdot H_2O + 2F_2 \rightarrow CrF_3 + N_2 + H_2O + 6HF \quad (5)$$

In line with this assumption, the second step starts when the approximate molar ratio between the added F_2 and the $[N_2H_6][CrF_5]\cdot H_2O$ precursor, exceeds 2, i.e. when the $[N_2H_6]^{2+}$ species are largely consumed. At this point, the solid consists of larger irregular pieces and some powder, and has a very low surface area of around 7 $m^2\,g^{-1}$. Interesting to note, similarly low surface areas in the range of 7–10 $m^2\,g^{-1}$ were obtained also from the anhydrous $[N_2H_5]_3[CrF_6]$ precursors. The bulk decomposition of the hydrazinium compound to CrF_3 (5) does therefore not yield products with high surface areas.

In the second step, the colour of the liquid phase changes to intense orange, while the solid disintegrates further into a fine and more homogeneous grass-green powder (Fig. 2 right). A small amount of the starting material can still be observed. After the bulk of the starting material has decomposed according to (5), part of the released H_2O, probably in the protonated form as $[H_3O]^+$, reacts with CrF_3 and with elemental F_2 to form CrO_2F_2:

$$2CrF_3 + 4H_2O + 3F_2 \rightarrow 2CrO_2F_2 + 8HF \quad (6)$$

In this step, the temperature of the reaction vessel does not increase after fluorine additions indicating that the processes are considerably less exothermic as in the first stage. In order to verify the CrO_2F_2 formation mechanism indicated by (6), a separate experiment under otherwise identical conditions was carried out with commercial $CrF_3\cdot 3.5H_2O$. After the addition of F_2, the colour of the initial dark green solution changed to almost colourless together with the formation of a grass-green powder and the solution above the green solid slowly turned into bright orange during the next 24 h. The orange compound could be extracted from the reaction vessel cooled to 223 K. The only chromium compound with significant vapour pressure at this temperature is CrO_2F_2. Identity of this compound was additionally confirmed by Raman spectroscopy; solidified extract showed bands at 957 and 937 cm^{-1}, which perfectly match the strongest bands of solid CrO_2F_2 at 955 and 935 cm^{-1} [28]. Formation of CrO_2F_2 gives therefore a clear evidence of a partial oxidation of Cr^{3+} to Cr^{6+}. In previous investigations, CrO_2F_2 was prepared at room temperature in quantitative yields when potassium chromate, K_2CrO_4, reacted with an excess of HF [32].

In the final stage, the orange solution with a grass-green solid is transformed into a brown-green solid with an almost colourless supernatant solution. Evidently, a partial conversion of CrO_2F_2 into some other $Cr^{>3+}$ components is taking place. As mentioned above, a reliable identification of these compounds could not be accomplished. Discolouration of the previously orange solution may be regarded as an additional indication of the presumed $CrOF_3$ formation. Namely, while CrO_2F_2 and $CrOF_4$ are both highly soluble, $CrOF_3$ is only slightly soluble in aHF [30].

However, the possible reaction pathways leading from CrO_2F_2 to $CrOF_3$ under the current circumstances remain unclear. There is apparently a lack of direct precedents in the available literature. In the reactions of CrO_2F_2 with F_2 at 473 K [33], or with KrF_2 in HF at 293 K [29], $CrOF_4$ was formed. Reaction of CrO_2F_2 with XeF_2 at 450 K yielded $CrOF_3$, possibly through the intermediate formation of $CrOF_4$ [34]. The original route to $CrOF_3$ included the reaction of either CrO_3 or CrO_2F_2 with ClF at 373 K followed by treating the intermediate $CrOF_3\cdot xClF$ with F_2 at 393 K [30]. On the other side, reaction between CrF_5 and H_2O, performed in a HF solvent at 298 K, resulted in $CrOF_3$ [35]. However, formation of CrF_5 also requires rather severe conditions, e.g. it was obtained from CrF_3 and F_2 at 533–623 K [35,36], or from $CrOF_3$ and F_2 at 463 K [30]. It appears that the latter reaction also proceeds via the $CrOF_4$ intermediate [37]. All indicated reactions of CrO_2F_2 and $CrOF_3$ take place at elevated temperatures, at room temperature only reactions with very reactive species, like KrF_2 or CrF_5, seem to take place. Under the conditions employed here, i.e. room temperature, moderate F_2 pressures, liquid aHF solvent/medium, and presence of H_2O, it is unlikely that these reactions are operative to a greater extent. In order to verify this, solution of CrO_2F_2 in aHF was left in contact with F_2 for 24 h either at room temperature or at 323 K. In both case, no reaction could be observed. The test at room temperature was repeated with the addition of a commercial anhydrous CrF_3. Even after one month, there were no signs of any reaction. It can be presumed that further reactions of CrO_2F_2 observed here can be influenced by the highly amorphous nanoscopic CrF_3 phase, reactivity of which can differ significantly from that of conventional macroscopic CrF_3 materials [38]. It is also possible that some residual species, like $[NH_4]^+$ and $[H_3O]^+$, which partly resist oxidation at these conditions [25,39], as well as traces of unreacted $[N_2H_6]^{2+}$, possibly embedded in the solid matrix, may influence these processes, especially when the relatively long timescale of the current experiments is taken into consideration. However, the applied instrumental setup did not allow a more detailed investigation of these aspects.

2.3. Some properties of HS-CrF_3

In contrast to the HS-AlF_3, which was found to be partially nanocrystalline, the HS-CrF_3 was completely amorphous. As shown in preliminary transmission electron microscopy (TEM) screening, HS-CrF_3 consists of agglomerated rounded nanoparticles with the sizes down to 5–10 nm, for which the diffuse circles in the experimental selected area electron diffraction (SAED) patterns indicated the absence of any

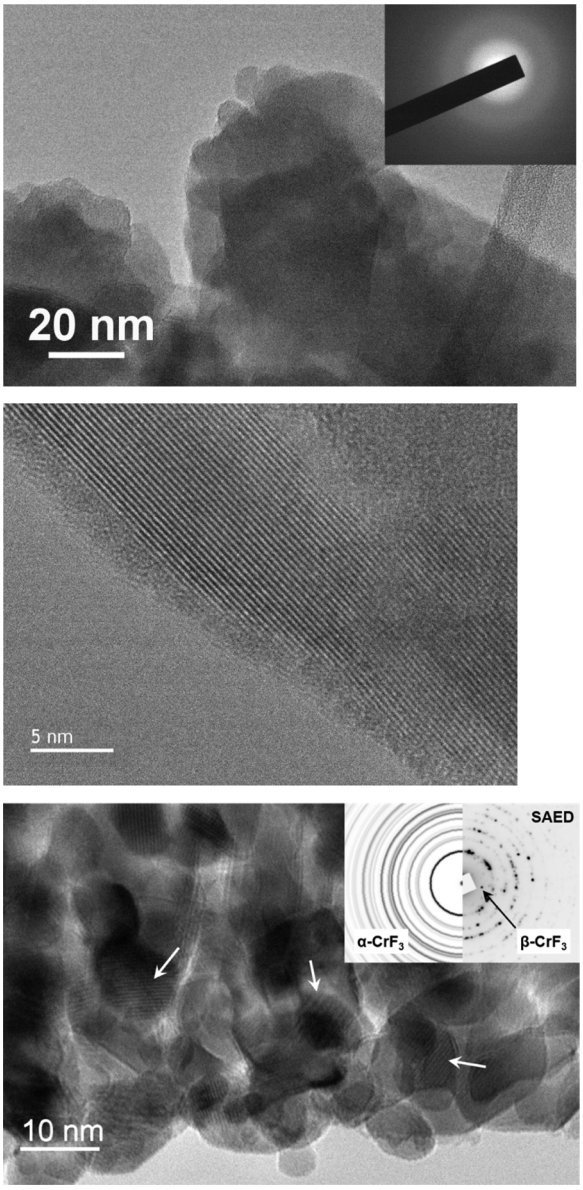

Fig. 3. TEM micrographs of HS-CrF_3 materials: typical nanostructure of HS-CrF_3, the inset experimental SAED pattern indicates a completely amorphous structure down to the nanolevel (top); extensive beam-induced ordering/crystallization of the metastable amorphous phase during TEM measurements (middle); crystallization within individual nanoparticles (white arrows) after catalytic test in CCl_2F_2 dismutation at 573 K, the inset experimental and calculated SAED patterns indicate the prevalent formation of the α-CrF_3 phase (bottom). (Top micrograph reproduced from Ref. [24] with permission from Elsevier).

structural order even at the nanoscale (Fig. 3 top) [24]. However, more detailed TEM studies confirm that these materials are metastable and are readily crystallized after longer beam-exposures, as shown in Fig. 3 (middle). Partial crystallization occurs also in materials used in catalytic tests, which are detailed below (Fig. 3 bottom).

The texture of the HS-CrF_3 products was determined by nitrogen (N_2) physisorption. A typical N_2 adsorption-desorption isotherm for these materials with the corresponding pore size distribution is presented in Fig. 4. The isotherm can be regarded as a combination of a Type I and Type II isotherms [40] with a considerable N_2 adsorption at low relative pressures (p/p°), and a rapid and non-limiting rise when p/p° is approaching unity. The Type I isotherms are typical for microporous solids, while the Type II isotherms are ascribed to non-porous or

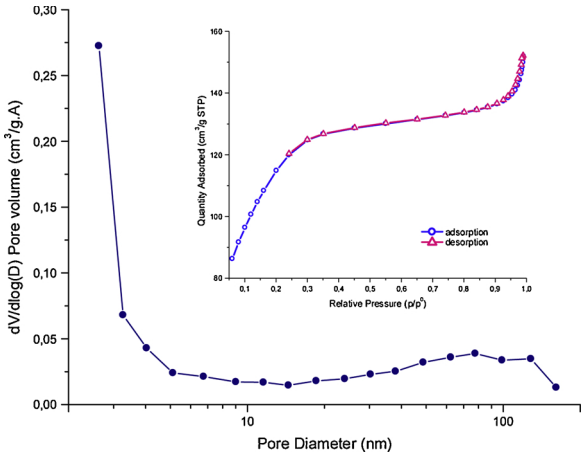

Fig. 4. Pore size distribution and nitrogen adsorption–desorption isotherm (inset) for the HS-CrF_3 with a BET surface area of 420 $m^2\,g^{-1}$.

macroporous solids. The resulting bimodal distribution of pores is shown in Fig. 4, and is in general consistent with TEM observations (Fig. 3 top and bottom). The pores below 5 nm prevail. The largest pores in this region very likely represent the interstices between the primary nanoparticles forming the densely packed larger agglomerates, while the smaller pores, i.e. the real micropores below 2 nm, are probably located also within the individual nanoparticles. On the other side, the macropores represent the larger empty spaces between the clusters of agglomerates. Considerable retention of residues in raw products pumped at room temperature (see Section 2.1.) can be, among other factors, attributed also to microporosity. Effective removal of HF and other volatile residues from such pores is accomplished only after prolonged treatment in vacuo at 523 K. In addition, it is very likely that removal of volatile chromium species, like CrO_2F_2 and eventually $CrOF_4$, creates additional microporosity within the nanoscopic CrF_3 matrix. This may be the main reason why the hydrated precursors yield HS-CrF_3 products, while the non-hydrated ones result in products with much lower surface areas.

Surface characteristics of HS-CrF_3 materials were investigated with photoacoustic FTIR spectroscopy (PAS) to determine their acidity, and in different model catalytic reactions of CFCs. The latter allow direct comparisons with the catalytic behaviour of chromium-based catalysts from preceding studies, e.g. [16,20]. PAS spectra of HS-CrF_3 obtained by evacuation of raw decomposition products at 523 K (Fig. 5 bottom) are in line with chemical analysis (Table 2) showing very low levels of residual $[NH_4]^+$, which exhibits a characteristic intense band at about 1445 cm^{-1} [25]. In the same spectrum, the broad peak at about 1630 cm^{-1}, attributed to the bending δ(H–O–H) mode of H_2O, indicates that some hydration is present. Pyridine (py) adsorption (Fig. 5 middle) reveals the presence of mainly Lewis acid sites with the most indicative bands at 1452 and 1615 cm^{-1}. However, the band at 1546 cm^{-1} indicates the presence of some Brønsted acid sites. As mentioned before for similarly prepared AlF_3 materials [25], the Brønsted sites in this type of fluorides may originate from residual oxygen-containing species, e.g. H_2O or $[H_3O]^+$, or from the short exposure of materials to ambient air before measurements. With the applied experimental procedure, a clear distinction between oxygen species from the two sources is therefore not possible. For the HS-CrF_3 materials, which were used in catalytic tests with either CCl_2F_2 or CCl_2FCClF_2 at temperatures up to 623 K a considerable incorporation of chlorine was observed (Table 2). Increase of chlorine content is accompanied by the decrease of fluorine content, still, the ratio of halogens versus chromium remains close to 3. This clearly indicates the replacement of fluorine with chlorine, i.e. chlorination of the CrF_3 to surprisingly high levels. The F/Cl exchange is a well-known process occurring on chromium catalysts and was extensively investigated in

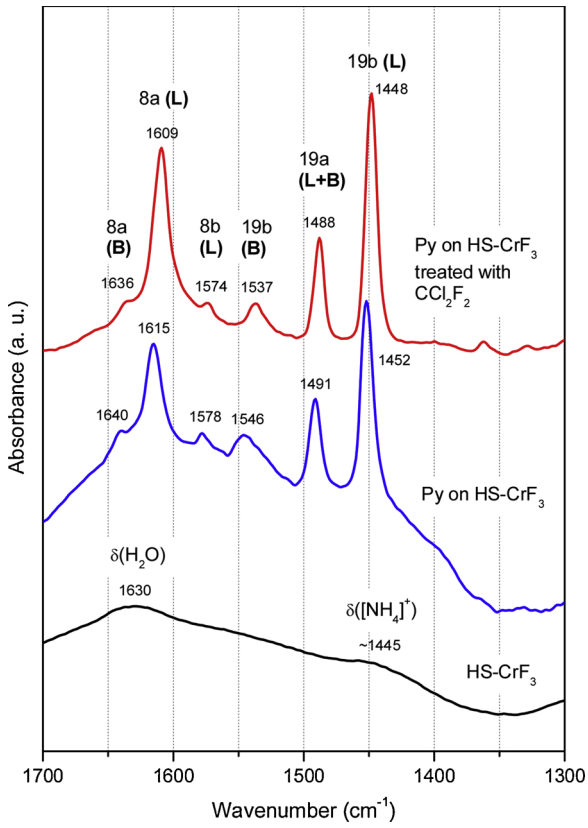

Fig. 5. Photoacoustic IR spectra of: HS-CrF_3 (bottom), after adsorption of pyridine (py) (middle), after adsorption of py on HS-CrF_3 that was treated with CCl_2F_2 at 573 K (top). Upper two tracks: the markings denote the vibration modes of pyridine adsorbed on Lewis (L) or Brønsted (B) acid sites [41].

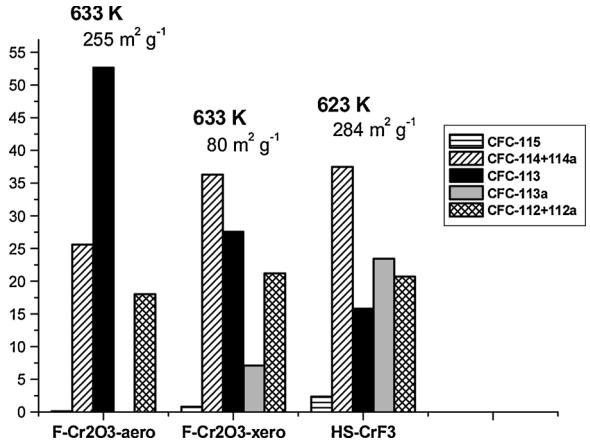

Fig. 6. Catalytic reaction of CCl_2FCClF_2 (CFC-113) on HS-CrF_3 compared to that on Cr_2O_3-based aerogel (F-Cr_2O_3-aero) and xerogel (F-Cr_2O_3-xero), both pre-fluorinated with CHF_3 [16]. Figures indicate the respective temperatures and the BET surface areas. Contact time in all indicated catalytic tests was 1 s. CFC code: 115 – $CClF_2CF_3$; 114 – $CClF_2CClF_2$; 114a – CCl_2FCF_3; 113 – CCl_2FCClF_2; 113a – CCl_3CF_3; 112 – CCl_2FCCl_2F; 112a – CCl_3CClF_2.

the past [2]. Majority of the previous work was however done on fluorinated chromia catalysts that can contain significant amounts of the unconverted Cr_2O_3 matrix. Chlorine incorporation into such materials can be, depending on the specific conditions used, described as a typical F/Cl exchange process [42], or as an additional chlorination of the Cr_2O_3 matrix [20], or combination of both. Chlorination of the present HS-CrF_3 materials with CFCs can be considered a classical F/Cl exchange between the fluorine in the almost completely fluorinated solid and the chlorine in CFCs. Until the equilibrium is reached, HS-CrF_3 acts as a fluorinating agent for the CFCs, while CFCs are chlorinating agents for the CrF_3. It should be noted that these processes apparently lead to lower Lewis acidity. PAS of the HS-CrF_3 after catalytic tests shows a distinctive shift of the characteristic py bands to lower wavenumbers (Fig. 5 top). Fluorine for chlorine exchange taking place during the heterogeneous catalytic reactions results therefore in the formation of Lewis acid sites, which are weaker as those found in the original HS-CrF_3. In the initial stages of the reaction, in the so-called activation period, CFCs are also involved in the reduction of $Cr^{>3+}$ to Cr^{3+}. Chemical analysis of the HS-CrF_3 used in catalytic tests with CCl_2F_2 shows a nearly tenfold reduction of the Cr^{6+} content (Table 2). On the other side, a complete reduction of Cr^{6+} is achieved when HS-CrF_3 is treated with acetone at 523 K, while the initial F/Cr ration of 3 remains unchanged (Table 2). Earlier, a vigorous reaction between $CrOF_3$ and acetone was reported [30]. In a subsequent study [37], no reaction between $CrOF_3$ and dry acetone was observed, however, a violent reaction occurred when small, but unspecified, amounts of H_2O were present.

In addition, the surface area of HS-CrF_3 materials used in catalytic tests dropped from 284 $m^2 g^{-1}$ to 169 $m^2 g^{-1}$ after tests with CCl_2F_2, and to 193 $m^2 g^{-1}$ after tests with CCl_2FCClF_2 (Table 2). Reduction of the surface area seems to correlate with the extent of chlorination. TEM investigations of HS-CrF_3 used in CCl_2F_2 dismutation (Fig. 3 bottom) reveal a partial crystallization within individual nanoparticles. This process is apparently not accompanied by excessive grain growth. Comparison of experimental and calculated SAED patterns indicates the prevalent formation of the nanocrystalline α-CrF_3 phase. However, there are some indications that some β-CrF_3 phase may also be present. Reduction of surface area can therefore be ascribed to several factors, like partial replacement of F^- ions with larger Cl^- ions, loss of some microporosity, and beginning of ordering/crystallization on the nanoscopic level. Catalytic activity of the newly prepared HS-CrF_3 materials was tested in two model reactions with CFCs performed under steady flow conditions, dismutation of CCl_2F_2, and reactions with CCl_2FCClF_2. In line with the exhibited Lewis acidity (Fig. 5), HS-CrF_3 is active in both test reactions that are known to proceed only on catalysts with sufficiently strong Lewis acid sites. In CCl_2F_2 dismutation; conversion of CCl_2F_2 at 423 K was 16.0% while at 523 K it reached 86.8%. Reaction of CCl_2FCClF_2 in contact with HS-CrF_3 showed distinctive differences when compared with some conventional Cr-based materials investigated earlier (Fig. 6). Overall conversion of CCl_2FCClF_2 and formation of the asymmetric isomer, CCl_3CF_3, were both noticeably higher for HS-CrF_3 than for conventional F-Cr_2O_3 materials in the form of either aerogel or xerogel [16]. Levels of the CCl_3CF_3 isomer obtained under steady flow conditions with HS-CrF_3 were similar to those observed in previous tests with F-Cr_2O_3 aerogels under very long contact times [20], suggesting a higher activity of the present HS-CrF_3 catalysts. Comparison with the F-Cr_2O_3 aerogel having a similarly high surface area (Fig. 6) implies that high activity of HS-CrF_3 cannot be related solely to the high surface area of the newly prepared materials. As shown by previous studies [43], treatment of chromia with CFCs or HFCs may strongly increase its Lewis acidity due to the two simultaneous processes, i.e. reduction of surface $Cr^{>3+}$ sites and their halogenation. As mentioned before, characterisation of the HS-CrF_3 materials indicates that they may contain up to 5 mass% of $CrOF_3$. According to chemical analyses, these species are reduced after CFC treatment and probably form very strong Lewis acid sites. Presence of the $Cr^{>3+}$ sites in current materials is therefore beneficial since it enables the formation of very active materials. From this aspect, HS-CrF_3 differs strongly from HS-AlF_3, in which the presence of side products, like the $[NH_4]^+$ compounds, strongly impaired their catalytic behaviour w.r.t. CCl_2FCClF_2 isomerization [25]. For both catalytic reactions, longer catalytic runs lead to a slow deactivation that may be a result of several

concurrent processes, like gradual chlorination of the solid with the associated reduction of Lewis acidity, partial crystallization and reduction of the surface area, and coke formation.

3. Conclusions

Decomposition of hydrazinium fluorometallates(III) with F_2 in aHF medium, which was originally developed as an entirely inorganic route to HS-AlF_3 materials [24,25], was successfully applied also in the preparation of HS-CrF_3 materials with unprecedented characteristics. Although the basic reaction mechanisms may appear similar, the two reaction systems differ significantly.

In contrast to HS-AlF_3, which was obtained from an anhydrous precursor, the HS-CrF_3 products are attainable exclusively from the hydrated precursor, $[N_2H_6][CrF_5]\cdot H_2O$. Reaction of the latter with F_2 in aHF medium proceeds in at least two consecutive steps: (i) in the initial stage, oxidative decomposition of the cationic part in the precursor, $[N_2H_6]^{2+}$, with F_2 takes place and gives a CrF_3 intermediate with low surface area, (ii) the following stage includes oxidation of some Cr^{3+} to $Cr^{>3+}$, reaction with residual $H_2O/[H_3O]^+$ species, and formation of chromium fluoride oxides, CrO_2F_2 and, very likely, $CrOF_3$. The final HS-CrF_3 with surface areas in the range of 180–420 $m^2\,g^{-1}$ is obtained after removal of residual volatile species, mainly HF, CrO_2F_2, and $[NH_4]F$, at moderate conditions. By this means, the nanoscopic character of the basic particles is retained, and microporosity is formed.

Despite its nanoscopic nature, exceptionally high surface area, and pronounced microporosity, the bulk composition of the newly prepared HS-fluoride is remarkably close to the stoichiometric CrF_3. The main residual by-product is supposed to be the non-volatile fluoride oxide, $CrOF_3$, which is the main source of $Cr^{>3+}$ and oxygen in the final product. Other residual species, like H_2O, $[H_3O]^+$, OH^-, and $[NH_4]^+$, are present in much lower amounts. Although the exact mass balance of oxygen could not be defined, the results indicate that the water from the hydrated precursor is almost quantitatively decomposed to volatile products and effectively removed from the reaction system as O_2 (4), and, partly, in the form of volatile chromium fluoride oxides, e.g. as CrO_2F_2 (6). In addition, removal of volatile chromium species from the amorphous CrF_3 matrix generates microporosity. This appears to be the key step in the formation of HS-CrF_3.

The newly prepared HS-CrF_3 materials exhibit Lewis acidity and are consequently very active catalysts in the investigated model reactions with some CFCs. High reactivity of these solids towards CFCs is evidenced by a substantial incorporation of chlorine because of the F/Cl exchange reactions between the CFC molecules and the solid fluoride. Observed reactivity of HS-CrF_3 materials is the result of their exceptionally high surface area and high purity. These materials consist mainly of CrF_3, and minor amounts of the $CrOF_3$ by-product. Presence of the latter is apparently not problematic, since the in-situ reduction and halogenation of the related $Cr^{>3+}$ sites with CFCs very likely produce additional Lewis acidic sites. On the other side, content of species, which could block or interfere with the active sites, like $H_2O/[H_3O]^+$ or $[NH_4]^+$, is comparatively very low. In addition, these materials, although metastable, can be employed at temperatures up to 623 K without losing their nanoscopic character. For these reasons, the HS-CrF_3 could be employed as an interesting new benchmark material for mechanistic and catalytic investigations in fluorocarbon chemistry.

4. Experimental

4.1. Preparation procedures

4.1.1. Synthesis of the $[N_2H_6][CrF_5]\cdot H_2O$ precursor

Synthesis of the starting materials was performed according to a modified procedure described earlier [44]. All preparation steps were carried out in polyethylene beakers. The $[N_2H_6]F_2$ was synthesized by slow addition of a 20% aqueous solution of HF (diluted 40% hydrofluoric acid, Riedel-de Haën) into a 40% aqueous solution of N_2H_4 (diluted 80% solution of hydrazine hydrate, Riedel-de Haën). White crystalline product was obtained which was dried at 333 K (Calculated for $[N_2H_6]F_2$: N_2H_4, 44.4%; F_t, 52.8%; Found: N_2H_4, 43.5%; F_t, 52.0%). Metal chromium (powder 99.99%, Alfa Aesar) was dissolved in a 40% aqueous solution of HF. Solution of $[N_2H_6]F_2$ in water was added into the acidic chromium fluoride solution in a stoichiometrical ratio of 1:1. The clear green solution was evaporated on water bath at 313 K, after that the crystalline product was dried at 323 K (Calculated for $[N_2H_6][CrF_5]\cdot H_2O$: N_2H_4, 16.1%; F_t, 47.7%; Cr, 26.1%; Found: N_2H_4, 16.2%; F_t, 47.0%; Cr, 25.6%;).

4.1.2. Preparation of HS-CrF_3

CAUTION! The following preparation procedures include the use of anhydrous hydrogen fluoride (aHF) and fluorine (F_2). Both chemicals are highly toxic and potentially dangerous. They must be handled with high precaution by using appropriate apparatus and protective clothing.

Volatile materials (F_2, aHF) were handled in an all-PTFE vacuum line equipped with PTFE valves. Manipulation of the non–volatile materials was done in a dry box at H_2O levels below 1 ppm (M. Braun). Small scale reactions (up to 4 g of starting material) were carried out in fluorinated ethylene propylene (FEP, copolymer of hexafluoropropylene and tetrafluoroethylene) reaction vessels (height 250–300 mm, ID/OD of 15.5/18.7 mm, Fig. 2) equipped with PTFE valves and PTFE coated stirring bars. Larger scale reactions (over 4 g of starting material) were carried out in modified round bottom 500 ml flasks made of FEP, which were equipped with PTFE valves and PTFE coated stirring bars. Prolonged use of the latter led to some contamination with PTFE shavings (e.g. Table 2), especially in larger batches which were stirred for several weeks. In some experiments, the stirring bars were therefore not used all the time. In these cases, adequate agitation within the reaction vessel was attained on a laboratory shaker. Prior to use, all lines and vessels were passivated with elemental fluorine. Fluorine was used as supplied (98%, Solvay). Anhydrous HF (Purum, Fluka) was pre-treated with K_2NiF_6 (Ozark Mahoning) for several hours.

In a typical preparation, the solid precursor, $[N_2H_6][CrF_5]\cdot H_2O$, was weighted in a dry box into a FEP reaction vessel. The vessel was connected to a vacuum line, evacuated, and cooled to 77 K with liquid N_2. The required amount of aHF, employed in the current preparations as a solvent and a medium, was condensed into the cooled vessel. After aHF addition, the vessel was warmed-up to room temperature. The green colour of the formed liquid phase (Fig. 2 left) indicates that the starting material is slightly soluble in liquid aHF. Relatively large quantities of the aHF solvent were employed to assure homogeneity, to increase the heath capacity of the reaction medium, and to prevent potentially dangerous local overheating, which may result from the strongly exothermic reaction between F_2 and the unwetted precursor particles. Thereafter, F_2 was dosed in several portions into the reaction vessel kept at room temperature. In the initial, strongly exothermic stages of the reaction (5), smaller portions of F_2 were added (up to 120 kPa of F_2 at room temperature). The course of reaction was monitored by measuring the pressure inside the reaction vessel after cooling it to 77 K. When the pressure in the cooled vessel was different from that of F_2 at this temperature, i.e. approx. 36 kPa, the reaction was considered to be not completed and the volatiles were pumped out at 77 K. Afterwards, the vessel was warmed-up to room temperature again and a new portion of F_2 was added at room temperature. In the final stages, larger doses of F_2 were added, but not higher than 320 kPa of F_2 at room temperature. Each F_2 portion was allowed to react with the strongly agitated reaction mixture for at least two days before a new portion of F_2 was added. After the reaction was completed, the raw product was isolated at room temperature by pumping out the residual gasses and aHF. Altogether, an approximate 33% excess of F_2 was

added according to the stoichiometrical ratio of 3 (4). The weight of the raw product was always higher than stoichiometrically predicted due to the retention of some aHF and the formation of small amounts of volatile $Cr^{>3+}$ species (see Section 2.1). The final HS-CrF_3 product was obtained after the raw product was additionally dried in vacuo at 523 K for at least 20 h.

The CrO_2F_2 used in some experiments was synthesized from K_2CrO_4 and aHF according to the published procedure [32].

4.2. Chemical analysis

The total fluorine (F_t) and total chlorine (Cl_t) contents were determined after complete decomposition of the sample by alkali fusion using $KNaCO_3$ [45,46]. The F_t content was determined by fluoride ion selective electrode [45,47], and the Cl_t content by precipitation titration with $Hg(NO_3)_2$ [48]. The content of Cr^{6+} was determined spectrophotometrically [49], while the total chromium (Cr_t) content was determined after complete oxidation of chromium by redox titration with $Fe(SO_4)_2$ [50]. The content of $[NH_4]^+$ was determined spectrophotometrically after distillation from alkaline media [48,49]. The PTFE content was determined by weighing the floating insoluble residue, which was found after dissolution of products in water.

4.3. Raman spectroscopy

Raman spectra of powdered samples were recorded in sealed quartz capillaries on a Raman Imaging Microscope System 1000 (Renishaw) by using the 632.8 nm excitation line of the He-Ne laser. Geometry for all the Raman experiments was 180° backscattering with laser power of 25 mW.

4.4. Infrared (IR) measurements

Infrared (IR) spectra were recorded on a Spectrum GX Fourier transform IR spectrometer (PerkinElmer) equipped with a Model 300 photoacoustic detector (MTEC). During the transfer to the photoacoustic cell, samples were for a short time exposed to ambient air. Pyridine (py) adsorption followed by photoacoustic spectroscopy of chemisorbed py (PAS-py) were performed according to the procedure reported earlier [20,41]. Before py adsorption at 423 K, samples were conditioned in a flow of N_2 at 523 K for 1 h.

4.5. Nitrogen pysisorption

Nitrogen (N_2) physisorption measurements were carried out at liquid-N_2 temperature, 77 K, by means of a FlowSorb II 2300 or a Gemini VII 2390 t instruments (both from Micromeritics). Specific surface area was determined either by a 1-point Brunauer-Emmett-Teller (BET) method on a FlowSorb instrument, or by a 5-point BET method on a Gemini instrument. The isotherms and the corresponding pore size distributions were determined by the Gemini instrument using the Barrett-Joyner-Halenda (BJH) method. Before analysis, each sample was degassed in vacuo (9 Pa) at 523 K for 2 h.

4.6. Transmission electron microscopy (TEM)

The transmission electron microscopy (TEM) was performed on JEM 2100 electron microscope (JEOL). The powders were placed on the Ni-C grid in a dry-box and the exposure to ambient air during the transfer into the microscope was kept at the minimum. Because of the observed beam-sensitivity of the current materials, all investigations were done using the smallest condenser aperture and spot size. Experimental selected-area electron diffraction (SAED) patterns were compared to calculated (simulated) patterns in order to identify the crystal structure of the phases [51]. Simulated patterns were calculated using the Electron Microscopy Image Simulation Package (EMS) program [52].

4.7. Catalytic tests

Catalytic behaviour of the newly prepared HS-CrF_3 was examined under steady flow conditions with a catalytic rig similar to that used in previous investigations of fluorinated or fluoride aluminium- or chromium-based materials [16,25,53]. Reaction conditions and test protocols were similar to those used in the indicated previous investigations to facilitate comparisons. Both starting substances, CCl_2F_2 and $CClF_2CCl_2F$, were diluted with N_2 to 20 vol.%. Flow of CCl_2F_2 was regulated directly by a mass flow controller, while the $CClF_2CCl_2F$ was dosed from a thermostated saturator. Catalytic tests were performed with a fixed bed of catalyst in a tubular catalytic reactor made of nickel. The products were analysed on-line by gas chromatography.

Acknowledgements

The Slovenian Research Agency (ARRS), Slovenia is acknowledged for funding this work within the research program P1-0045 Inorganic Chemistry and Technology, and within the research project J2-7319 Direct Conversion of Methane to Higher Hydrocarbons Using Superacid Catalysts. The authors are also obliged to Asst. Prof. Andreja Benčan Golob for TEM measurements, and to Dr. Aleš Štefančič for some spectrometric and catalytic measurements.

References

[1] E. Kemnitz, D.-H. Menz, Fluorinated metal oxides and metal fluorides as heterogeneous catalysts, Prog. Solid State Chem. 26 (1998) 97–153.
[2] E. Kemnitz, J.M. Winfield, Fluoride catalysts: their application to heterogeneous catalytic fluorination and related processes, in: T. Nakajima, A. Tressaud, B. Žemva (Eds.), Advanced Inorganic Fluorides: Synthesis, Characterization and Applications, Elsevier Science S. A., Lausanne, 2000, pp. 367–402.
[3] D. Lennon, J.M. Winfield, Heterogeneous catalysts used for large-scale syntheses of selected chlorohydrocarbons and fluorohydrocarbons: fluorinated chromia and eta-alumina, in: V.I. Parvulescu, E. Kemnitz (Eds.), New Materials for Catalytic Applications, Elsevier B.V., 2016, pp. 193–217.
[4] D.W. Bonniface, J.R. Fryer, P. Landon, J.D. Scott, W.D.S. Scott, M.J. Watson, G. Webb, J.M. Winfield, Halogen exchange reactions for CFC alternatives. The behaviour of fluorine-18 labelled hydrogen fluoride towards prefluorinated chromia containing nickel(II) or zinc(II), Green Chem. 1 (1999) 9–11.
[5] K.-U. Niedersen, E. Schreier, E. Kemnitz, Isomerization reaction of 1,1,2,2-tetrafluoroethane on chromia - A study of the active sites on the surface, J. Catal. 167 (1997) 210–214.
[6] L.Q. Xing, Q.Y. Bi, Y.J. Wang, M. Guo, J.Q. Lu, M.F. Luo, In situ Raman spectroscopy studies on chromium oxide catalyst in an anhydrous hydrogen fluoride atmosphere, J. Raman Spectrosc. 42 (2011) 1095–1099.
[7] M. Nappa, S. Peng, X. Sun, Industrial syntheses of hydrohaloolefins and related products, in: H. Groult, F.R. Leroux, A. Tressaud (Eds.), Modern Synthesis Processes and Reactivity of Fluorinated Compounds, Elsevier Inc., 2017, pp. 27–69.
[8] K. Teinz, S.R. Manuel, B.B. Chen, A. Pigamo, N. Doucet, E. Kemnitz, Catalytic formation of 2,3,3,3-tetrafluoropropene from 2-chloro-3,3,3-trifluoropropene at fluorinated chromia: a study of reaction pathways, Appl. Catal. B: Environ. 165 (2015) 200–208.
[9] W. Mao, B. Wang, Y. Ma, W. Zhang, Y. Du, Y. Qin, J. Kang, J. Lu, Selective gas-phase catalytic fluorination of 1,1,2,3-tetrachloropropene to 2-chloro-3,3,3-trifluoropropene, Catal. Commun. 49 (2014) 73–77.
[10] W. Han, Z. Wang, X. Li, H. Tang, M. Xi, Y. Li, H. Liu, Solution combustion synthesis of nano-chromia as catalyst for the dehydrofluorination of 1,1-difluoroethane, J. Mater. Sci. 51 (2016) 11002–11013.
[11] S. Lim, M.S. Kim, J.-W. Choi, H. Kim, B.S. Ahn, S.D. Lee, H. Lee, C.S. Kim, D.J. Suh, J.-M. Ha, K.H. Song, Catalytic dehydrofluorination of 1,1,1,2,3-pentafluoropropane (HFC-245eb) to 2,3,3,3-tetrafluoropropene (HFO-1234yf) using in-situ fluorinated chromium oxyfluoride catalyst, Catal. Today 293-294 (2017) 42–48.
[12] J.-W. Luo, J.-D. Song, W.-Z. Jia, Z.-Y. Pu, J.-Q. Lu, M.-F. Luo, Catalytic dehydrofluorination of 1,1,1,3,3-pentafluoropropane to 1,3,3,3-tetrafluoropropene over fluorinated NiO/Cr_2O_3 catalysts, Appl. Surf. Sci. 433 (2018) 904–913.
[13] C.P. Zhang, X.Q. Jia, H.D. Quan, Synthesis of Z-1,1,1,4,4,4-hexafluoro-2-butene from hexachlorobutadiene, J. Fluorine Chem. 191 (2016) 77–83.
[14] R.Z. Hu, C.P. Zhang, F.Y. Qing, H.D. Quan, Synthesis of 2,3,3,3-tetrafluoropropene via vapor-phase catalytic fluorination in the presence of Cr-based catalyst, J. Fluorine Chem. 185 (2016) 187–190.
[15] E. Ünveren, E. Kemnitz, U. Oran, W.E.S. Unger, Static TOF-SIMS surface analysis of a CCl_2F_2 activated chromia catalyst used for a Cl/F exchange reaction, J. Phys. Chem. B 108 (2004) 15454–15456.
[16] H. Bozorgzadeh, E. Kemnitz, M. Nickkho-Amiry, T. Skapin, J.M. Winfield, Catalytic reactions of chlorofluoroethanes at fluorinated alumina and chromia aerogels and xerogels - A comparison of reaction pathways in alumina- and chromia-based catalysts, J. Fluorine Chem. 110 (2001) 181–189.

[17] H.D. Quan, H.E. Yang, M. Tamura, A. Sekiya, Synthesis of a porous chromium fluoride catalyst with a large surface area, J. Catal. 231 (2005) 254–257.
[18] X.Q. Jia, H.D. Quan, M. Tamura, A. Sekiya, Synthesis of microporous fluorinated chromia with a sharp pore distribution, RSC Adv. 2 (2012) 6695–6700.
[19] T. Skapin, E. Kemnitz, Fluorination effects in chromia aerogels and xerogels, J. Non-Cryst, Solids 225 (1998) 163–167.
[20] H. Bozorgzadeh, E. Kemnitz, M. Nickkho-Amiry, T. Skapin, J.M. Winfield, Dynamic behaviour of chlorofluoroethanes at fluorinated chromia aerogels and fluorinated zinc(II) or magnesium(II) doped chromia aerogels, J. Fluorine Chem. 121 (2003) 83–92.
[21] E. Kemnitz, A. Kohne, I. Grohmann, A. Lippitz, W.E.S. Unger, X-ray photoelectron and X-ray excited auger electron spectroscopic analysis of surface modifications of chromia during heterogeneous catalyzed chlorine fluorine exchange, J. Catal. 159 (1996) 270–279.
[22] B. Adamczyk, O. Boese, N. Weiher, S.L.M. Schroeder, E. Kemnitz, Fluorine modified chromium oxide and its impact on heterogeneously catalyzed fluorination reactions, J. Fluorine Chem. 101 (2000) 239–246.
[23] G. Scholz, E. Kemnitz, Sol–gel synthesis of metal fluorides: reactivity and mechanisms, in: H. Groult, F.R. Leroux, A. Tressaud (Eds.), Modern Synthesis Processes and Reactivity of Fluorinated Compounds, Elsevier Inc., 2017, pp. 609–649.
[24] T. Skapin, G. Tavčar, A. Benčan, Z. Mazej, Recent developments in the preparation of high surface area fluorides, J. Fluorine Chem. 130 (2009) 1086–1092.
[25] T. Skapin, Z. Mazej, A. Makarowicz, A. Jesih, M. Nickkho-Amiry, S.L.M. Schroeder, N. Weiher, B. Žemva, J.M. Winfield, Aluminium(III) fluoride originating from decomposition of hydrazinium fluoroaluminate(III) under oxidative conditions: syntheses, X-ray photoelectron spectroscopy and some catalytic reactions, J. Fluorine Chem. 132 (2011) 703–712.
[26] J. Slivnik, J. Maček, A. Rahten, B. Sedej, Thermal-properties of hydrazinium fluorometallates of the first row transition elements, Thermochim. Acta 39 (1980) 21–33.
[27] U. Bentrup, On the thermal decomposition of $N_2H_6[CrF_5(H_2O)]$ and the new compound $N_2H_6CrF_5$, Z. Naturforsch. 47b (1992) 957–961.
[28] S.D. Brown, G.L. Gard, T.M. Loehr, Chemistry of chromyl fluoride. IV. Raman spectrum of CrO_2F_2 in the solid and liquid phases, J. Chem. Phys. 64 (1976) 1219–1222.
[29] K.O. Christe, W.W. Wilson, R.A. Bougon, Synthesis and characterization of CrF_4O, $KrF_2{\cdot}CrF_4O$, and $NO^+CrF_5O^-$, Inorg. Chem. 25 (1986) 2163–2169.
[30] P.J. Green, B.M. Johnson, T.M. Loehr, G.L. Gard, Chromium oxide trifluoride ($CrOF_3$), Preparation and properties, Inorg. Chem. 21 (1982) 3562–3565.
[31] G.E. Walrafen, P.N. Krishnan, Raman-spectrum of pressure compacted fused-silica, J. Chem. Phys. 74 (1981) 5328–5330.
[32] A.K. Brisdon, J.H. Holloway, E.G. Hope, Mild fluorination of oxo-anions; a clean route to Group 6 and 7 transition metal oxide fluorides, J. Fluorine Chem. 89 (1998) 35–37.
[33] J.F. Huang, K. Hedberg, J.M. Shreeve, S.P. Mallela, Gas-phase molecular-structure of chromium oxytetrafluoride, $CrOF_4$, Inorg. Chem. 27 (1988) 4633–4635.
[34] M. McHughes, R.D. Willett, H.B. Davis, G.L. Gard, Chromium oxide trifluoride ($CrOF_3$). Preparation and crystal structure, Inorg. Chem. 25 (1986) 426–427.
[35] R. Bougon, W.W. Wilson, K.O. Christe, Synthesis and characterization of NF_4CrF_6 and reaction chemistry of CrF_5, Inorg. Chem. 24 (1985) 2286–2292.
[36] J. Slivnik, B. Žemva, Reactions of chromium(V) fluoride with xenon and xenon difluoride, Z. Anorg. Allg. Chem. 385 (1971) 137–141.
[37] E.G. Hope, P.J. Jones, W. Levason, J.S. Ogden, M. Tajik, J.W. Turff, Synthesis and properties of chromium(V) trifluoride oxide $CrOF_3$ and related oxo-anions, J. Chem. Soc. Dalton Trans. (1984) 2445–2447.
[38] S. Rüdiger, U. Groß, E. Kemnitz, Non-aqueous sol-gel synthesis of nano-structured metal fluorides, J. Fluorine Chem. 128 (2007) 353–368.
[39] M. Gerken, M.D. Moran, H.P.A. Mercier, B.E. Pointner, G.J. Schrobilgen, B. Hoge, K.O. Christe, J.A. Boatz, On the XeF^+/H_2O system: synthesis and characterization of the xenon(II) oxide fluoride cation, $FXeOXeFXeF^+$, J. Am. Chem. Soc. 131 (2009) 13474–13489.
[40] K.S.W. Sing, D.H. Everett, R.A.W. Haul, L. Moscou, R.A. Pierotti, J. Rouquerol, T. Siemieniewska, Reporting physisorption data for gas/solid systems with special reference to the determination of surface area and porosity, Pure Appl. Chem. 57 (1985) 603–619.
[41] A. Hess, E. Kemnitz, Characterization of catalytically active sites on aluminum oxides, hydroxyfluorides, and fluorides in correlation with their catalytic behavior, J. Catal. 149 (1994) 449–457.
[42] A. Farrokhnia, B. Sakakini, K.C. Waugh, Kinetic and mechanistic study of the reaction of CCl_4 with prefluorided chromia to form CCl_3F and CCl_2F_2, J. Catal. 174 (1998) 219–230.
[43] D.R. Coulson, P.W.J.G. Wijnen, J.J. Lerou, L.E. Manzer, Chromium oxide-catalyzed disproportionation of chlorodifluoromethane: a mechanism study, J. Catal. 140 (1993) 103–120.
[44] P. Bukovec, Fluoro metallates(III). 6. Hydrazinium(1^+ and 2^+)-fluoro chromates (III), Monatsh. Chem. 105 (1974) 517–524.
[45] M. Ponikvar, B. Sedej, B. Pihlar, B. Žemva, Determination of fluoride in $M(SbF_6)_X$ compounds, Anal. Chim. Acta 418 (2000) 113–118.
[46] M. Nečemer, P. Kump, M. Rajčevič, R. Jačimović, B. Budič, M. Ponikvar, Determination of sulfur and chlorine in fodder by X-ray fluorescence spectral analysis and comparison with other analytical methods, Spectrochim. Acta B 58 (2003) 1367–1373.
[47] M. Ponikvar, B. Žemva, J.F. Liebman, The analytical and descriptive inorganic chemistry of the hydrolysis of hexafluoropnictate ions, PnF_6^- (Pn = P, As, Sb, Bi), J. Fluorine Chem. 123 (2003) 217–220.
[48] A.I. Vogel, Vogel's Textbook of Quantitative Inorganic Analysis: Including Elementary Instrumental Analysis, 4th ed., Longman, London, 1978, pp. 346–347.
[49] HACH DR/2010 Spectrophotometer Handbook.
[50] N.H. Furman, Standard methods of chemical analysis (Vol. 1), 6th ed., D. Van Nostrand Company, Princeton, 1962, pp. 366–368.
[51] S. Javorič, G. Dražič, M. Kosec, A study of the crystallization of CSD-prepared $La_{0.5}Sr_{0.5}CoO_3$ thin films using analytical electron microscopy, J. Eur. Ceram. Soc. 21 (2001) 1573-1546.
[52] P.A. Stadelmann, EMS – a software package for electron-diffraction analysis and HREM image simulation in materials science, Ultramicroscopy 21 (1987) 131–145.
[53] H. Bozorgzadeh, E. Kemnitz, M. Nickkho-Amiry, T. Skapin, J.M. Winfield, Conversion of 1,1,2-trichlorotrifluoroethane to 1,1,1-trichlorotrifluoroethane and 1,1-dichlorotetrafluoroethane over aluminium-based catalysts, J. Fluorine Chem. 107 (2001) 45–52.